Available online at www.sciencedirect.com
ScienceDirect
Trans. Nonferrous Met. Soc. China 30(2020) 3347−3355
Transactions of Nonferrous Metals Society of China
www.tnmsc.cn

A simple physical mixing method for MnO_2/MnO nanocomposites with superior Zn^{2+} storage performance

Xiao-bei ZANG[1], Ling-tong LI[1], Zhi-xin SUN[1], Rabah BOUKHERROUB[2], Jia-xin MENG[1], Kun-peng CAI[1], Qing-guo SHAO[1], Ning CAO[1]

1. School of Materials Science and Engineering, China University of Petroleum (East China), Qingdao 266580, China;
2. University Lille, CNRS UMR 8520-IEMN, Lille, F-59000, France

Received 18 February 2020; accepted 28 September 2020

Abstract: MnO_2/MnO cathode material with superior Zn^{2+} storage performance is prepared through a simple physical mixing method. The MnO_2/MnO nanocomposite with a mixed mass ratio of 12:1 exhibits the highest specific capacity (364.2 mA·h/g at 0.2*C*), good cycle performance (170.4 mA·h/g after 100 cycles) and excellent rate performance (205.7 mA·h/g at 2*C*). Analysis of cyclic voltammetry (CV) data at various scan rates shows that both diffusion-controlled insertion behavior and surface capacitive behavior contribute to the Zn^{2+} storage performance of MnO_2/MnO cathodes. And the capacitive behavior contributes more at high discharge rates, due to the short paths of ion diffusion and the rapid transfer of electrons.

Key words: zinc-ion battery; MnO_2/MnO cathode material; physical mixing method; reaction kinetics

1 Introduction

At present, lithium-ion batteries (LIBs) play a dominant role in the rechargeable battery market, due to the high energy density and long cycle life. LIBs are widely used in the fields of portable mobile devices, electric vehicles, and power storage aspects (wind, hydraulic and solar power) [1−3]. Unfortunately, the further development of LIBs is seriously restrained by the limited lithium resources, safety issues caused by organic electrolytes and strict assembly conditions [4]. Therefore, it is urgent to find alternative rechargeable batteries featuring high safety, abundant raw materials, low cost and great capability. Zinc-ion batteries (ZIBs), which consist of Zn anode, mild aqueous electrolyte and cathode material, could well overcome the afore-said drawbacks, and therefore are attracting more and more attention. The energy storage of ZIBs is based on the insertion/extraction of Zn^{2+} into/from cathode material [5]. Zn anode has high theoretical capacity (820 mA·h/g, 5855 mA·h/cm^3) and low redox potential (−0.76 V vs SHE) [6], so exploring potential satisfactory cathode materials for Zn^{2+} insertion is key to the development of ZIBs.

So far, Mn-based materials [7−9], V-based materials [10−12], and Prussian blue analogues [13] have been mainly applied in cathode materials of ZIBs. Among them, Mn-based materials receive extensive attention due to their high theoretical capacity and suitable discharge voltage [14]. The reported Mn-based cathodes are mainly concentrated on MnO_2 with a single Mn valence (+4). Unfortunately, MnO_2 has poor conductivity and large volume change during charge and discharge process, which affects rate performance

Foundation item: Project (21905304) supported by the National Natural Science Foundation of China; Project (ZR2019BEM031) supported by the Natural Science Foundation of Shandong Province, China; Projects (18CX02158A, 19CX05001A) supported by the Fundamental Research Funds for the Central Universities, China
Corresponding author: Ning CAO; Tel: +86-15376713767; E-mail: caoning@upc.edu.cn
DOI: 10.1016/S1003-6326(20)65466-8

and cycle life of ZIBs. Many methods have been developed to improve the performance of MnO_2 cathodes, normally by fabricating nanostructured forms (nanoflakes [7], nanorods [8], nanospheres [15], etc) and doping with conductive materials (carbon nanotubes [16], graphene [17], etc). Although these methods have greatly improved the rate capability and cycle life of MnO_2 cathode, the complicated preparation process and high cost make them unsuitable for mass production.

As known to all, Mn has multiple oxidation states (+2, +3, +4, +6, and so on). Recently, some researchers have studied the properties of mixed valence manganese oxides. It was found that the coexistence of Mn in different valence states can result in good catalytic oxidation activity [18,19], anomalously high specific capacitance, excellent power density and long cycling life [20,21].

Herein, we prepared a high performance MnO_2/MnO cathode using a simple physical mixing method. The morphology, phase structure and storage mechanism of MnO_2/MnO cathode were analyzed through scanning electron microscopy (SEM), X-ray diffraction (XRD), Brunauer−Emmett−TellerInstrument (BET) characterization and electrochemical measurements.

2 Experimental

2.1 Materials

Various manganese oxides used in this experiment were purchased from Shanghai Macklin Biochemical Technology Co., Ltd, China. The purities of MnO_2, MnO, Mn_2O_3 and Mn_3O_4 are 99.95%, 99%, 98% and 97%, respectively.

2.2 Material characterization

The crystal structure of samples was characterized by XRD (D8 Advance, Bruker) employing Cu K_α radiation from 10° to 80°. The micromorphology was observed by SEM (SU8100, Hitachi). The specific surface area and pore size were obtained by BET (ASAP 2460, Micromeritics).

2.3 Electrochemical measurement

The CR2032 coin cells were assembled with Zn foil as anode, glass fiber as separator, and aqueous solution containing 2 mol/L $ZnSO_4$ and 0.1 mol/L $MnSO_4$ as electrolyte. The cathode was composed of 80 wt.% active materials (manganese oxides), 10 wt.% conductive material (acetylene black), and 10 wt.% binding agent (polyvinylidene fluoride, PVDF) in N-methyl-2-pyrrolidone (NMP). The slurry was cast onto stainless steel foil after being stirred evenly. The electrode was dried at 80 °C for 10 h and then cut into disks of 12 mm in diameter (the typical active material loading was about 0.8−1 mg/cm^2).

The rate and cycle performances were measured on LAND battery measurement system (CT3001K) with a voltage window from 1 to 1.9 V at various current rates (0.2−2)*C*. For Zn−MnO_2 batteries, 1*C* is approximately equal to 617 mA/g. CV measurements were carried out using an electrochemical workstation (ModuLab XM) under the voltage ranging from 1 to 1.9 V at different scan rates (0.5−3 mV/s).

3 Results and discussion

3.1 Characterizations of manganese oxides

As shown in Fig. 1, the XRD diffractions display the crystal structures of various manganese oxides used in this study. The diffraction peaks of MnO, MnO_2, Mn_2O_3 and Mn_3O_4 can be well indexed to cubic MnO (JCPDS No. 07-0230; space group: $Fm\bar{3}m$), tetragonal β-MnO_2 (JCPDS No. 24-0735; space group: *P*42/*mnm*), cubic Mn_2O_3 (JCPDS No. 41-1442; space group: *Ia*-3), and tetragonal Mn_3O_4 (JCPDS No. 24-0734; space group: $I4_1/amd$). They are vastly different in their morphology, as observed by SEM. Except for the irregular bulk of MnO_2, MnO, Mn_2O_3 and Mn_3O_4 are respectively presented as angular nanospheres (~1 μm in diameter), small nanoparticles (~100 nm in diameter) and slender nanorods (~1 um in length) (Fig. 2).

The electrochemical performance of the four manganese oxides is illustrated in Fig. 3(a). The initial discharge specific capacities of MnO_2, MnO, Mn_2O_3 and Mn_3O_4 respectively correspond to 81.3, 42.3, 31.6 and 11.7 mA·h/g at 2*C*. Three mixtures of MnO_2/MnO, MnO_2/Mn_2O_3 and MnO_2/Mn_3O_4 nanocomposites were prepared as cathode active materials of ZIBs at a mass ratio of 1:1. From the electrochemical results in Fig. 3(b), MnO_2/MnO nanocomposite (1:1), MnO_2/Mn_2O_3 nanocomposite (1:1) and MnO_2/Mn_3O_4 nanocomposite (1:1) achieve a reversible capacity of 122.2, 87.5 and 55.6 mA·h/g at 2*C*, respectively. It can be easily

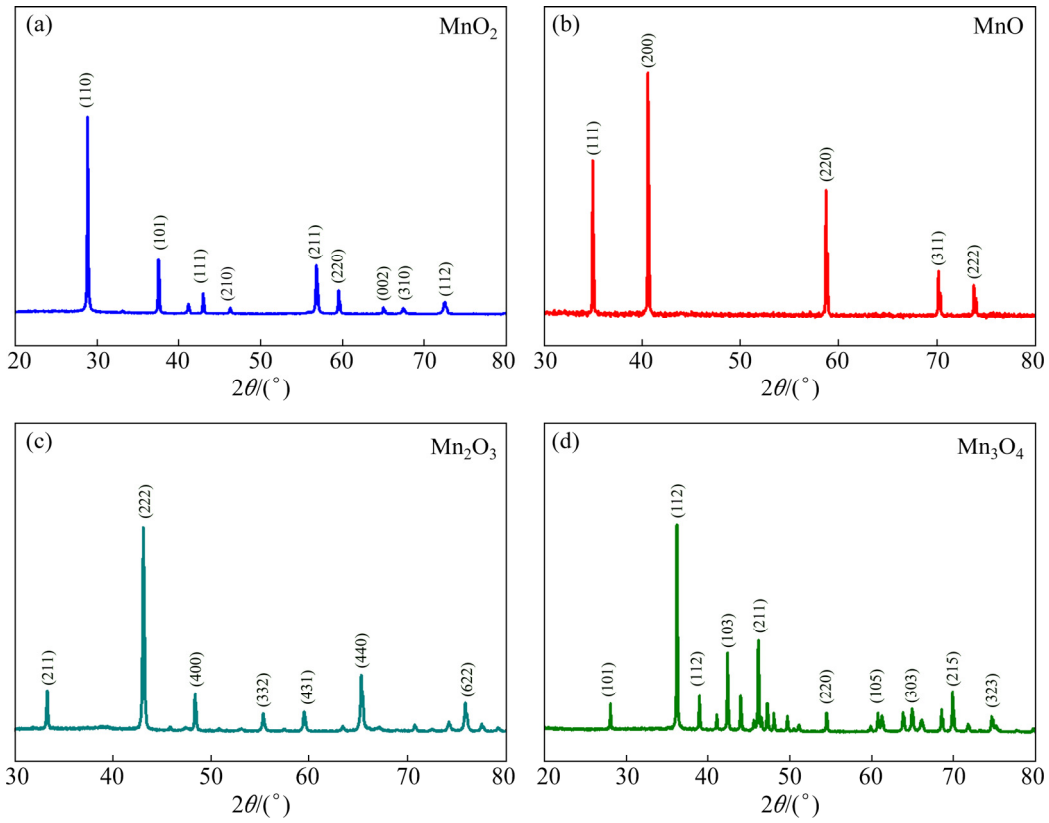

Fig. 1 XRD patterns of MnO_2 (a), MnO (b), Mn_2O_3 (c) and Mn_3O_4 (d)

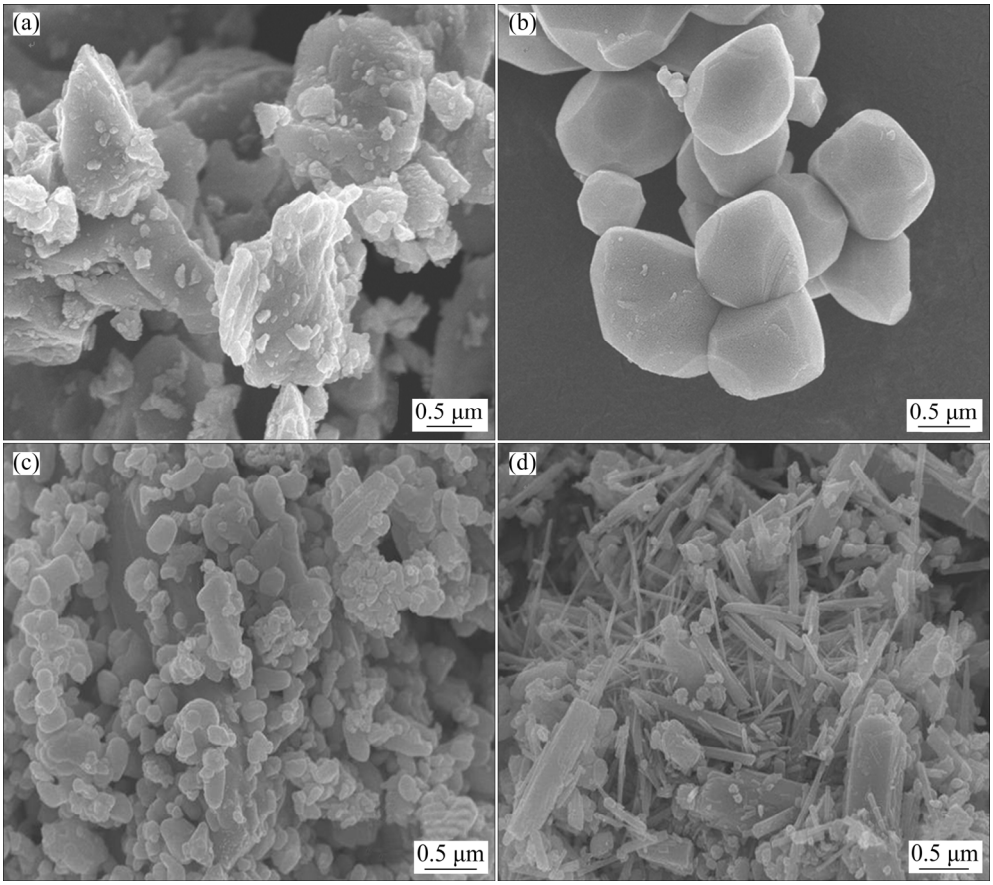

Fig. 2 SEM images of MnO_2 (a), MnO (b), Mn_2O_3 (c) and Mn_3O_4 (d)

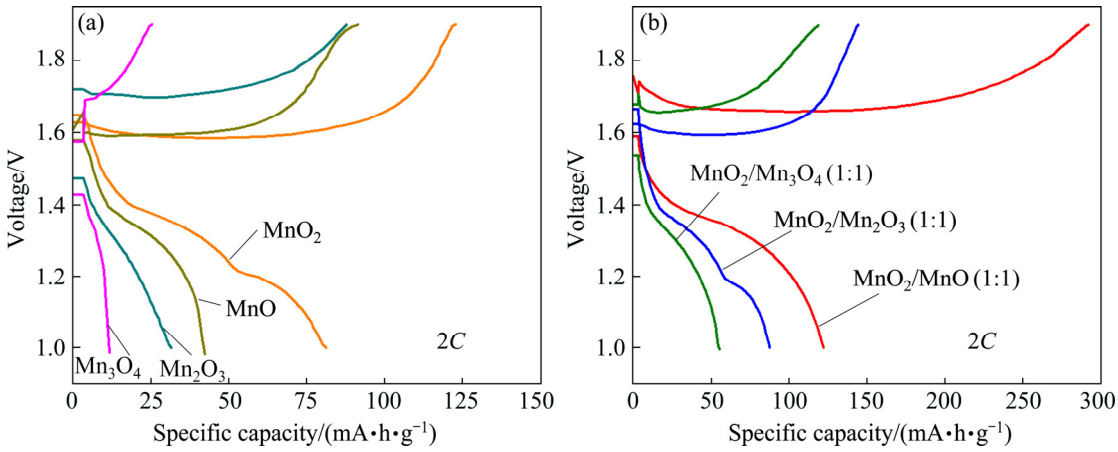

Fig. 3 Initial charge and discharge performance of cathodes: (a) MnO_2, MnO, Mn_2O_3 and Mn_3O_4; (b) MnO_2/MnO (1:1), MnO_2/Mn_2O_3 (1:1) and MnO_2/Mn_3O_4 (1:1)

found that the mixture of different manganese oxides could improve the specific capacity of ZIBs, especially the mixture of MnO_2 and MnO. In order to further improve the electrochemical properties, the MnO_2/MnO mass ratios are adjusted.

3.2 Effect of mass ratio on performance of MnO_2/MnO nanocomposites

In MnO_2/MnO nanocomposites, MnO_2 nanoparticles are distributed on the surface of angular MnO nanospheres (Figs. 4(a, b)), and the mixture of the two manganese oxides is further confirmed by XRD (Fig. 5). As a result, the architecture of angular nanospheres and small nanoparticles forms the mesoporous and macroporous structure of MnO_2/MnO nanocomposite with a concentrated pore size distribution of 2−100 nm (Fig. 6), and this porous structure is very likely to facilitate the transfer of Zn^{2+}. In addition, the introduction of MnO enhances the adhesion between electrode materials and current collector, and relieves the phenomenon of MnO_2 detachment.

Then, the electrochemical properties are tested. By performing five charge−discharge cycles at different rates, the highest specific capacities of MnO_2/MnO nanocomposites with different mixing mass ratios are compared in Fig. 7(a). It can be clearly seen that the discharge specific capacity of the MnO_2/MnO nanocomposite with a mass ratio of 12:1 is much higher than that of nanocomposites with other ratios, with specific capacity values of 364.2, 325.8, 314.9, 282.9, 205.7 mA·h/g at a rate of 0.2*C*, 0.5*C*, 0.7*C*, 1*C* and 2*C*, respectively (Fig. 7(b)). Compared with both MnO_2 cathode and

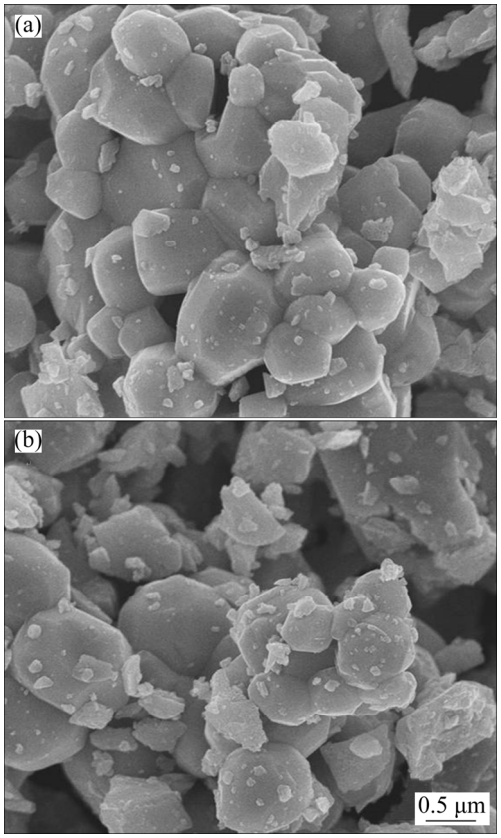

Fig. 4 SEM images of MnO_2/MnO (1:1) (a) and MnO_2/MnO (12:1) (b) nanocomposites

MnO cathode, the electrochemical performance of MnO_2/MnO (12:1) cathode is greatly improved. Surprisingly, the addition of MnO can nearly double the discharge specific capacity of the commonly used MnO_2 electrode (Fig. 7(c)). With the increase of the number of cycles, the discharge specific capacity of cathode materials firstly increases and then decreases (Fig. 7(d)). This phenomenon is commonly found in transition metal oxide

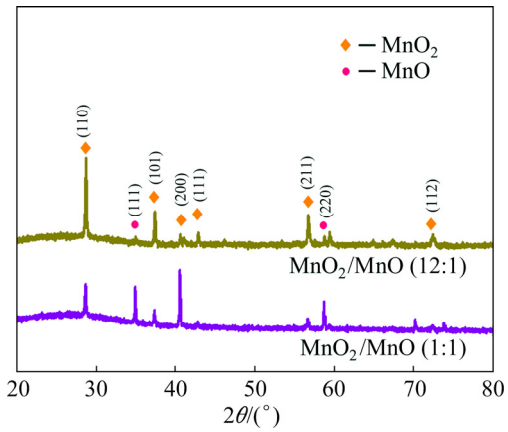

Fig. 5 XRD patterns of MnO_2/MnO nanocomposites

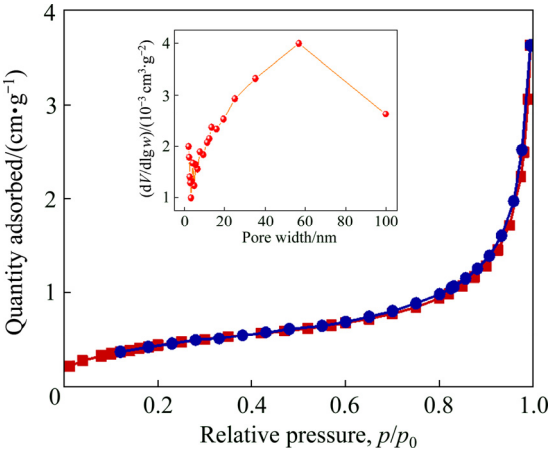

Fig. 6 N_2 adsorption/desorption isotherm of MnO_2/MnO nanocomposite (12:1) (Insert is corresponding pore size distribution)

electrodes, which is mainly caused by the slow electrochemical activation process [22]. Besides, MnO_2/MnO shows better electrochemical activity than MnO_2 and MnO, which is probably related to the high catalytic activity of mixed valence compounds [23]. The MnO_2/MnO cathode displays good cycling stability, while the discharge specific capacity decreases to 170.4 mA·h/g after 100 cycles.

Although MnO_2/MnO cathode exhibits better electrochemical performance than other typical cathode materials (Fig. 8) [17,24−28], it is also of great practical significance to conduct more research to extend the cycle life.

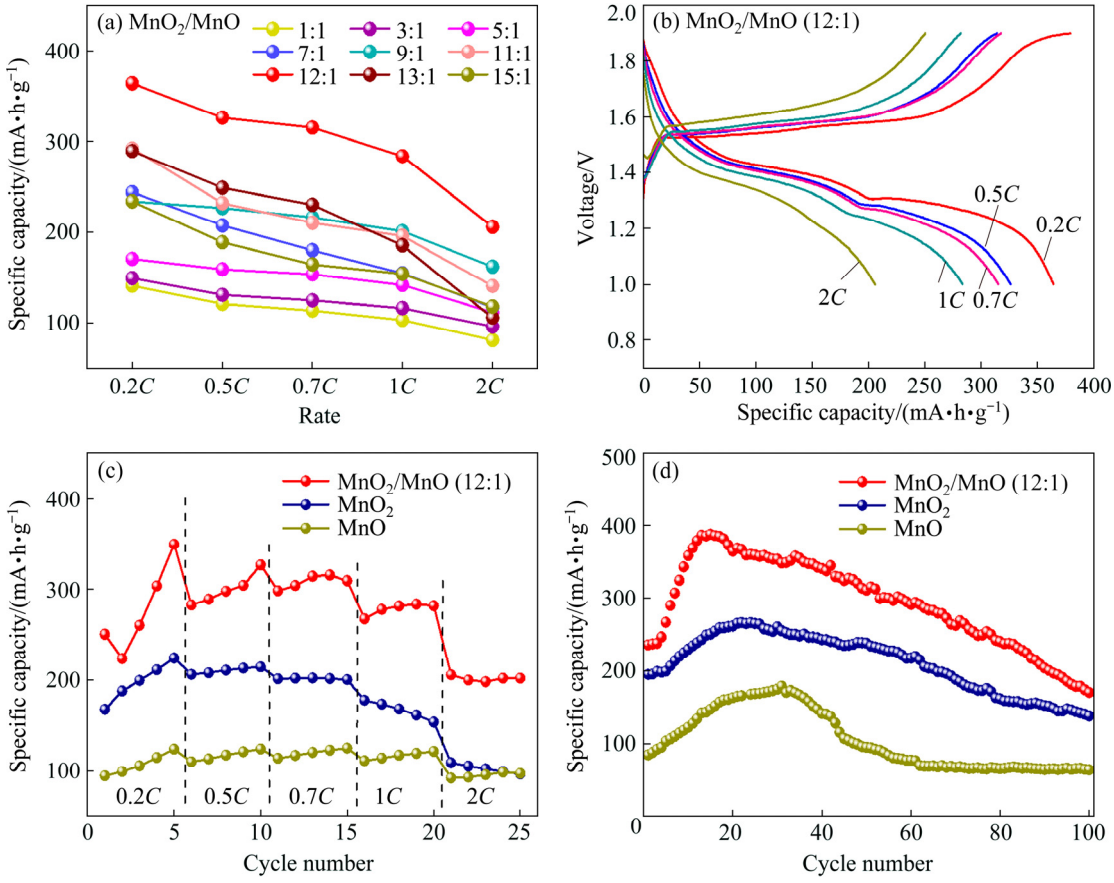

Fig. 7 Discharge specific capacity of MnO_2/MnO electrodes with different mixing ratios at different rates (a), charge and discharge curves of MnO_2/MnO (12:1) electrode at different rates (b), rate performance of MnO_2/MnO (12:1), MnO_2 and MnO electrodes (c), and cycle performance of MnO_2/MnO (12:1), MnO_2 and MnO electrodes (d)

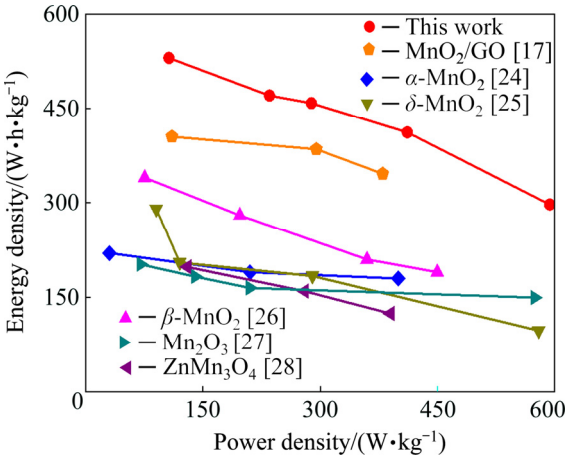

Fig. 8 Comparison between MnO_2/MnO cathode and other cathode materials reported

3.3 Energy-storage mechanism of MnO_2/MnO cathode

To further explore the energy-storage mechanism, CV curve of MnO_2/MnO electrode at a scan rate of 0.5 mV/s was used to analyze the transformation of MnO_2/MnO (Fig. 9(a)). In scans

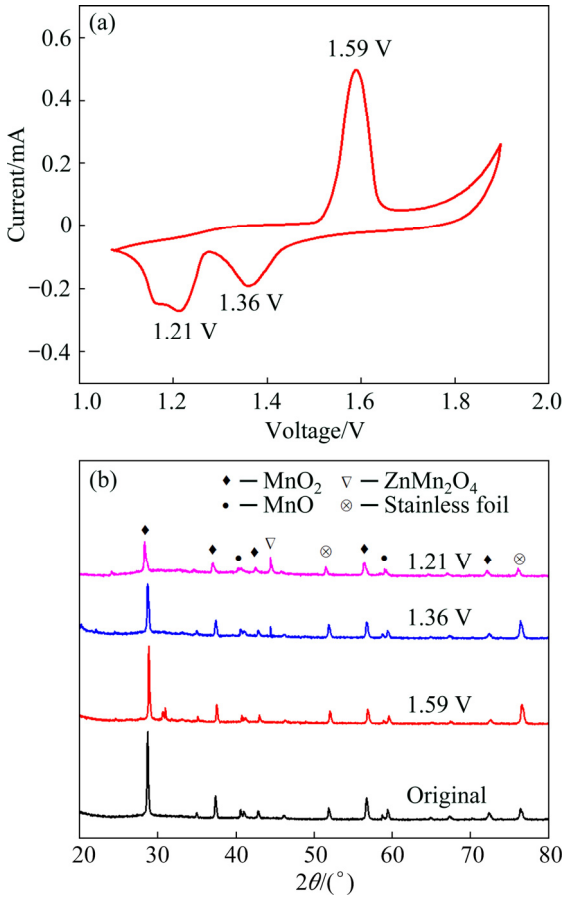

Fig. 9 CV curves of MnO_2/MnO electrode at 0.5 mV/s (a) and XRD patterns at redox peaks (b)

of the cathode, two reduction peaks are observable at 1.36 and 1.21 V, which can be ascribed to the insertion of Zn^{2+} into MnO_2/MnO hosts. In anodic scans, one oxidation peak is observed at 1.59 V, corresponding to the Zn^{2+}-extraction from MnO_2/MnO cathode. This is supported by the XRD analysis in Fig. 9(b). $ZnMn_2O_4$ is formed at the two reduction peaks and the composition is similar to the original one at the oxidation peak. The reactions of ZIBs during charge and discharge process can be summarized by Eqs. (1)−(3) and depicted as Fig. 10.

$$\text{Anode: } Zn \rightleftharpoons Zn^{2+}+2e \quad (1)$$

$$\text{Cathode: } MnO_2/MnO+Zn^{2+}+2e \rightleftharpoons ZnMn_2O_4 \quad (2)$$

$$\text{Overall: } MnO_2/MnO+Zn \rightleftharpoons ZnMn_2O_4 \quad (3)$$

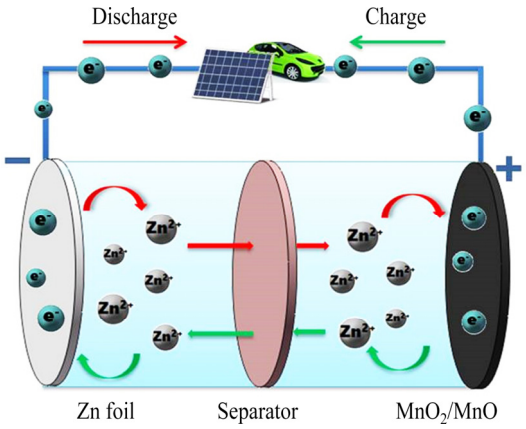

Fig. 10 Schematic illustration of ZIBs based on MnO_2/MnO cathode

To better understand fundamental mechanisms underlying the improved electrochemical performance of MnO_2/MnO electrode, the reaction kinetics were investigated by CV measurements. The CV measurements of MnO_2/MnO electrode (Fig. 11(a)) were carried out at various scan rates ranging from 0.5 to 3 mV/s. CV curves at various scan rates can help to understand the reversibility of the electrode reactions. Obviously, as the scan rate increases, the peaks on CV curves gradually become broader, but the shapes of CV curves remain consistent. The CV data at various scan rates are analyzed according to the following equations [22]:

$$I=av^b \quad (4)$$

where the current I conforms to a power law relationship with the sweep rate v. a and b are two adjustable parameters, and b values can be

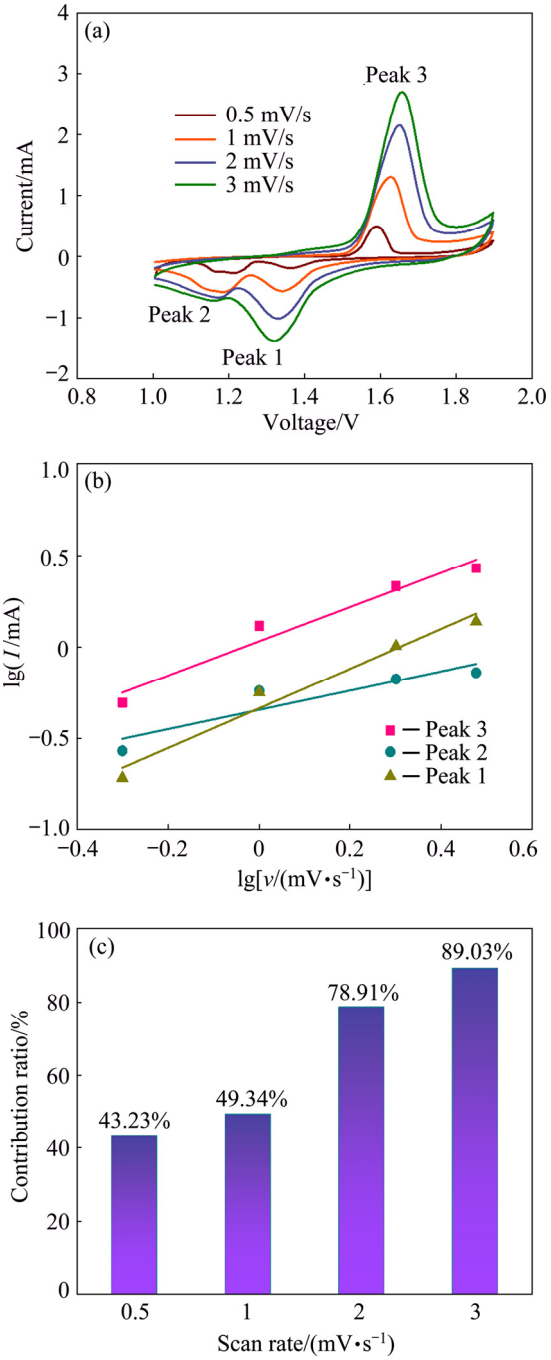

Fig. 11 CV curves of MnO_2/MnO electrode at different scan rates (a), lg I and lg v plots at specific peak currents (b), and contribution ratios of capacitive behavior to MnO_2/MnO electrode (c)

determined from the slope of the plot of lg I versus lg v, as described in the following equation:

$$\lg I=b\lg v+\lg a \quad (5)$$

where the coefficient b usually varies from 0.5 to 1. The b value of 0.5 indicates the diffusion-controlled insertion behavior, while the b value of 1 represents the surface capacitive behavior. As shown in Fig. 11(b), the b values of three redox peaks are calculated to be 1.09 (Peak 1), 0.534 (Peak 2) and 0.93 (Peak 3), respectively. It is suggested that both diffusion-controlled behavior and capacitive behavior contribute to the electrochemical kinetic of MnO_2/MnO electrode, but the capacitive behavior plays more important role. The specific contributions of capacitive behavior to the total capacity at various scan rates can be determined by

$$I(v)=k_1v+k_2v^{1/2} \quad (6)$$

where k_1v and $k_2v^{1/2}$ respectively represent the current contributions from surface capacitive behavior and diffusion-controlled insertion behavior. The calculation results in Fig. 11(c) show that the contribution of capacitive behavior increases gradually with the incremental scan rate. Specifically, the diffusion-controlled insertion behavior holds a dominant position in the total contribution of MnO_2/MnO electrode at low discharge rates, while capacitive behavior contributes more at high discharge rates. In conclusion, one of the reasons for the outstanding performance of MnO_2/MnO electrode at high rates can be attributed to the short paths of ion diffusion and the rapid transfer of electrons.

4 Conclusions

(1) The MnO_2/MnO nanocomposites have been successfully fabricated via a simple physical mixing. The SEM analyses reveal that MnO_2 nanoparticles are distributed on the surface of angular MnO nanospheres.

(2) The MnO_2/MnO cathode displays improved specific capacity values of 364.2 mA·h/g at the rate of 0.2C and excellent cycle stability versus commonly used MnO_2 cathode. And the optimized mass ratio of MnO_2/MnO is found to be 12:1.

(3) The mechanism of improved electrochemical performance is investigated by CV curve and reaction kinetics. The outstanding performance of MnO_2/MnO cathode at high rates is attributed to the short paths of ion diffusion and the rapid transfer of electrons.

References

[1] CHEN Q C, YAN G J, LUO L M, CHEN F, XIE T F, DAI S C, YUAN M L. Enhanced cycling stability of Mg−F

co-modified $LiNi_{0.6}Co_{0.2}Mn_{0.2-y}Mg_yO_{2-z}F_z$ for lithium-ion batteries [J]. Transactions of Nonferrous Metals Society of China, 2018, 28(7): 1397−1403. https://doi.org/10.1016/S1003-6326(18)64778-8.

[2] ZENG J, PENG C Q, WANG R C, LIU Y J, WANG X F, LIU J. Preparation of dual-shell Si/TiO_2/CFs composite and its lithium storage performance [J]. Transactions of Nonferrous Metals Society of China, 2019, 29(11): 2384−2391. https://doi.org/10.1016/S1003-6326(19)65144-7.

[3] YAN J, LIU W F, CHEN C, ZHAO C H, LIU K Y. Synthesis and characterization of porous monodisperse carbon spheres/selenium composite for high-performance rechargeable Li−Se batteries [J]. Transactions of Nonferrous Metals Society of China, 2018, 28(9): 1819−1827. https://doi.org/10.1016/S1003-6326(18)64826-5.

[4] FANG G Z, ZHOU J, PAN A Q, LIANG S Q. Recent advances in aqueous zinc-ion batteries [J]. ACS Energy Letters, 2018, 3: 2480−2501. https://doi.org/10.1021/acsenergylett.8b01426.

[5] XU D W, LI B H, WEI C G, HE Y B, DU H D, CHU X D, QIN X Y, YANG Q H, KANG F Y. Preparation and characterization of MnO_2/acid-treated CNT nanocomposites for energy storage with zinc ions [J]. Electrochimica Acta, 2014, 133: 254−261. https://doi.org/10.1016/j.electacta.2014.04.001.

[6] SONG M, TAN H, CHAO D L, FAN H J. Recent advances in zinc-ion batteries [J]. Advanced Functional Materials, 2018, 28: 1802564. https://doi.org/10.1002/adfm.201802564.

[7] ALFARUQI M H, ISLAM S, PUTRO D Y, MATHEW V, KIM S, JO J, KIM S, SUN Y K, KIM K, KIM J. Structural transformation and electrochemical study of layered MnO_2 in rechargeable aqueous zinc-ion battery [J]. Electrochimica Acta, 2018, 276: 1−11. https://doi.org/10.1016/j.electacta.2018.04.139.

[8] CHENG F Y, ZHANG J Z, SONG W N, LI C S, MA H, CHENG J, SHEN P W. Facile controlled synthesis of MnO_2 nanostructures of novel shapes and their application in batteries [J]. Inorganic Chemistry, 2006, 45: 2038−2044. https://doi.org/10.1021/ic051715b.

[9] CHEN L L, YANG Z H, QIN H G, ZENG X, MENG J L, CHEN H Z. Graphene-wrapped hollow $ZnMn_2O_4$ microspheres for high-performance cathode materials of aqueous zinc ion batteries [J]. Electrochimica Acta, 2019, 317: 155−163. https://doi.org/10.1016/j.electacta.2019.05.147.

[10] ZHOU J, SHAN L T, WU Z X, GUO X, FANG G Z, LIANG S Q. Investigation of V_2O_5 as a low-cost rechargeable aqueous zinc ion battery cathode [J]. Chemical Communications, 2018, 54(35): 4457−4460. https://doi.org/10.1039/C8CC02250J.

[11] LIU F, CHEN Z X, FANG G Z, WANG Z Q, CAI Y S, TANG B Y, ZHOU J, LIANG S Q. V_2O_5 nanospheres with mixed vanadium valences as high electrochemically active aqueous zinc-ion battery cathode [J]. Nano-micro Letters, 2019, 11: 1−11. https://doi.org/10.1007/s40820-019-0256-2.

[12] HE P, YAN M Y, ZHANG G B, SUN R M, CHEN L N, AN Q Y, MAI L Q. Layered VS_2 nanosheet-based aqueous Zn ion battery cathode [J]. Advanced Energy Materials, 2017, 7: 1601920. https://doi.org/10.1002/aenm.201601920.

[13] LIU Z, PULLETIKURTHI G, ENDRES F. A Prussian blue/zinc secondary battery with a bio-ionic liquid-water mixture as electrolyte [J]. ACS Applied Materials & Interfaces, 2016, 8: 12158−12164. https://doi.org/10.1021/acsami.6b01592.

[14] CHAO D L, ZHOU W H, YE C, ZHANG Q H, CHEN Y G, GU L, DAVEY K, QIAO S Z. An electrolytic Zn−MnO_2 battery for high-voltage and scalable energy storage [J]. Angewandte Chemie International Edition, 2019, 58: 7823−7828. https://doi.org/10.1002/anie.201904174.

[15] GUO X T, LI J M, JIN X, HAN Y H, LIN Y, LEI Z W, WANG S Y, QIN L J, JIAO S H, GAO R G. A hollow-structured manganese oxide cathode for stable Zn−MnO_2 batteries [J]. Nanomaterials, 2018, 8: 301. https://doi.org/10.3390/nano8050301.

[16] ZANG X B, HOU Y, WANG T, ZHANG R J, KANG F Y, ZHU H W. Temperature-resistant and flexible supercapacitors based on 10-inch wafer-scale nanocarbon films [J]. Science China Materials, 2019, 62: 947−954. https://doi.org/10.1007/s40843-018-9399-3.

[17] WU B K, ZHANG G B, YAN M Y, XIONG T F, HE P, HE L, XU X, MAI L Q. Graphene scroll-coated α-MnO_2 nanowires as high-performance cathode materials for aqueous Zn-ion battery [J]. Small, 2018, 14: 1703850. https://doi.org/10.1002/smll.201703850.

[18] TIAN Z, TONG W, WANG J, DUAN N, KRISHNAN V V, SUIB S L. Manganese oxide mesoporous structures: Mixed-valent semiconducting catalysts [J]. Science, 1997, 276: 926−930. DOI: 10.1126/science.276.5314.926.

[19] CHOU L Y, LIU R, HE W, HE S, GEH N, LIN Y J, HOU E Y F, WANG D W, HOU H J M. Direct oxygen and hydrogen production by photo water splitting using a robust bioinspired manganese-oxo oligomer complex/tungsten oxide catalytic system [J]. International Journal of Hydrogen Energy, 2012, 37: 8889−8896. https://doi.org/10.1016/j.ijhydene. 2012.02.074.

[20] WANG Y, LAI W H, WANG N, JIANG Z, WANG X Y, ZOU P C, LIN Z Y, FAN H J, KANG F Y, WONG C P, YANG C. A reduced graphene oxide/mixed-valence manganese oxide composite electrode for tailorable and surface mountable supercapacitors with high capacitance and super-long life [J]. Energy & Environmental Science, 2017, 10: 941−949. https://doi.org/10.1039/C6EE03773A.

[21] SONG M K, CHENG S, CHEN H Y, QIN W T, NAM K W, XU S C, YANG X Q, BONGIORNO A, LEE J S, BAI J M, TYSON T A, CHO J P, LIU M L. Anomalous pseudo-capacitive behavior of a nanostructured, mixed-valent manganese oxide film for electrical energy storage [J]. Nano Letters, 2012, 12: 3483−3490. https://doi.org/10.1021/nl300984y.

[22] QING F Y, WEI Q L, ZHANG G X, WANG X M, ZHANG J H, HU Y F, WANG D N, ZUIN L, ZHOU T, WU Y C, SUN S H. High-performance reversible aqueous Zn-ion battery based on porous MnO_x nanorods coated by MOF-derived N-doped carbon [J]. Advanced Energy Materials, 2018, 8: 1801445. https://doi.org/10.1002/aenm.201801445.

[23] TU J J, YANG Z D, HU C. Efficient catalytic aerobic oxidation of chlorinated phenols with mixed-valent manganese oxide nanoparticles [J]. Journal of Chemical

Technology & Biotechnology, 2015, 90: 80−86. https://doi.org/10.1002/jctb.4289.

[24] XU C J, LI B H, DU H D, KANG F Y. Energetic zinc ion chemistry: The rechargeable zinc ion battery [J]. Angewandte Chemie International Edition, 2012, 51: 933−935. https://doi.org/10.1002/anie.201106307.

[25] ALFARUQI M H, GIM J H, KIM S J, SONG J J, PHAM D T, JO J G, XIU Z L, MATHEW V, KIM J K. A layered δ-MnO_2 nanoflake cathode with high zinc-storage capacities for eco-friendly battery applications [J]. Electrochemistry Communications, 2015, 60: 121−125. https://doi.org/10.1016/j.elecom.2015.08.019.

[26] ZHANG N, CHENG F Y, LIU J X, WANG L B, LONG X H, LIU X S, LI F J, CHEN J. Rechargeable aqueous zinc-manganese dioxide batteries with high energy and power densities [J]. Nature Communications, 2017, 8: 405. https://doi.org/10.1038/s41467-017-00467-x.

[27] JIANG B Z, XU C J, WU C L, DONG L B, LI J, KANG F Y. Manganese sesquioxide as cathode material for multivalent zinc ion battery with high capacity and long cycle life [J]. Electrochimica Acta, 2017, 229: 422−428. https://doi.org/10.1016/j.electacta.2017.01.163.

[28] ZHANG N, CHENG F Y, LIU Y C, ZHAO Q, LEI K X, CHEN C C, LIU X S, CHEN J. Cation-deficient spinel $ZnMn_2O_4$ cathode in $Zn(CF_3SO_3)_2$ electrolyte for rechargeable aqueous Zn-ion battery [J]. Journal of the American Chemical Society, 2016, 138: 12894−12901. https://doi.org/10.1021/jacs.6b05958.

简单物理混合方法提高 MnO_2/MnO 纳米复合材料的储 Zn^{2+}性能

臧晓蓓[1]，李灵桐[1]，孙志欣[1]，Rabah BOUKHERROUB[2]，孟佳欣[1]，蔡鲲鹏[1]，邵庆国[1]，曹 宁[1]

1. 中国石油大学(华东) 材料科学与工程学院，青岛 266580；
2. University Lille, CNRS UMR 8520-IEMN, Lille, F-59000, France

摘 要：通过简单的物理混合方法制备具有优异储 Zn^{2+}性能的 MnO_2/MnO 正极材料。混合质量比为 12:1 的 MnO_2/MnO 纳米复合材料具有最高的比容量(0.2*C* 时达 364.2 mA·h/g)，良好的循环性能(100 次循环后达 170.4 mA·h/g)和倍率性能(2*C* 时达 205.7 mA·h/g)。通过探究储能机理，充放电过程中扩散控制的插入行为和表面电容行为均有助于 MnO_2/MnO 正极的储 Zn^{2+}性能。由于离子扩散的短路径和电子的快速转移，在高放电倍率下，电容行为发挥更大的作用。

关键词：锌离子电池；MnO_2/MnO 复合正极材料；物理混合方法；反应动力学

(Edited by Bing YANG)